Article

JOURNAL OF COMPOSITE MATERIALS

Journal of Composite Materials
2015, Vol. 49(1) 65–74

DOI: 10.1177/0021998313514261
jcm.sagepub.com

SAGE

A geometry-invariant fracture law for ceramic matrix composites

Konstantinos G Dassios

Abstract

This paper reports the development of a generalized fracture law that can assess the mechanical behavior of ceramic matrix composites (CMCs). The established law differs from conventional bridging laws in that it accounts not only for the bridging effect but also for all major energy dissipation mechanisms including matrix cracking and fiber pull-out. As such, the formulation can be used to directly assess the original, experimentally recorded, fracture behavior of the material in the load-extension domain. The established expression successfully approximated the experimental load versus beam deflection (P-u) curves of a SiC-fiber reinforced glass-ceramic matrix composite tested under the single-edge-notched beam (SENB) configuration. The fracture law was found to be geometry-invariant by comparison with results from tensile specimens with radically different damage zone geometries. A parametric analysis is presented which demonstrates the potential of the model in the *a priori* prediction of the fracture behavior of hypothetical CMCs with similar fracture characteristics.

Keywords

Ceramic matrix composites, bridging stresses, fracture, micromechanical modeling

Introduction

Silicon carbide (SiC) fibers are one of the most prominent types of reinforcement used in continuous fiber-reinforced ceramic matrix composite (CMC) materials, naturally predestined for high-temperature applications with increased thermo-mechanical performance demands in hostile oxidative environments.[1,2] The low density, high damage tolerance, and superior tribological properties of SiC-fiber reinforced CMCs are exploited today in applications such as aerospace and aircraft thermo-structural components, hot structures of launch vehicles, nose caps, nozzle jet vanes, engine flaps, and advanced friction systems.[3] Most of the desirable properties of such CMCs are a result of the crack propagation resistance offered by energy dissipation phenomena such as fiber bridging and pull-out that develop during their fracture.[4]

Due the dependence of conventional fracture mechanics descriptors, such as the crack growth resistance (*R*-curve), on specimen geometry and loading conditions, such analyses cannot constitutively approach the fracture behavior of CMCs.[5–7] A continuum approach is generally followed to intrinsically model such behaviors, by introducing a continuous bridging stress profile $\sigma_{br}(\delta)$, called the bridging law, where the bridging stresses depend on the local crack opening displacement δ.[8–11] While the bridging law approach is ideal for quantifying the contribution of the bridging phenomenon to the overall fracture behavior, a generalized expression that also considers the effect of matrix micro-cracking and pullout on the total energy dissipated during composite fracture has been proposed for simplified geometries and crack opening scenarios such as the tensile stretching of Double-Edge-Notched (DEN) specimens.[12] In the original formulation, the analytical expression of the generalized fracture law,

Department of Materials Science and Engineering, University of Ioannina, Greece

Corresponding author:
Konstantinos G Dassios, Department of Materials Science and Engineering, University of Ioannina, Ioannina GR-45110, Greece.
Email: kdassios@cc.uoi.gr

$\sigma(\delta)$, was expressed using the weakest link statistical concepts and rational boundary conditions as[12]

$$\sigma(\delta) = \frac{V_f}{l}\left\{\frac{1-V_f}{V_f}E_m\delta e^{-\left(\frac{\delta}{b_m}\right)^{a_m}} + E_f\delta e^{-\left(\frac{\delta}{b_f}\right)^{a_f}} + \frac{2klL_p\tau}{R_f}\left[e^{-\frac{\delta-\delta^*}{L_p}} - e^{-\frac{\delta-\delta^*}{L_p}-\left(\frac{\delta-\delta^*}{b_f}\right)^{a_f}}\right]\right\} \quad (1)$$

where k is the fraction of fibres effectively contributing to pull-out (e.g. $k = 0.5$, for a symmetrically stacked laminate) and the three terms within the brackets are the individual contributions of the matrix, intact fibers and pull-out fibers.

The purpose of this work is to provide a fracture law formulation that will be directly applicable to the loading configurations typically used for fracture toughness measurements – such as the single-edge-notched beam (SENB) specimen – where the bridging and damage zone constantly change shape during testing. Analytical and rational procedures are employed in order to establish an analytical expression for the load-deflection (P-u) behavior of the SENB geometry while keeping consistent with the micromechanics of damage developed for simple geometries. The resulting analytical expression was successful in assessing the experimental P-u curves of SENB specimens of different initial notch-to-width ratios within the pure-tension regime, i.e. before the appearance of compressive zone effects in the curve. The potential of the proposed law as a geometry-invariant fracture descriptor for CMCs is discussed in the text. A statistical analysis is also presented that shows how the law can be used to predict the P-u behavior of CMCs without the need of testing.

Experimental

Material

The composite material used in this study consists of silicon carbide (SiC) fibers, grade Nicalon (Nippon Carbon Co. Ltd., Japan), in a brittle glass-ceramic matrix. The weight stoichiometric composition of the fibers, which have been fabricated by pyrolytic polymerization of polycarbosilane, is 56.6% silicon, 31.7%, carbon and 11.7% oxygen. Table 1 presents major properties of the fibers, as reported by the manufacturer.

The glass-ceramic matrix was a mixture of magnesium oxide (MgO), aluminum oxide (Al_2O_3), silicon oxide (SiO_2), and lithium oxide (LiO_2), hereon denoted MASL. The matrix, initially prepared through the sol-gel route, was used to impregnate 12 laminated fiber preforms stacked in a symmetrical $[0/90]_s$ sequence. The final composite was received in the form of laminated plates of thickness 3.0 mm, after sintering at ~1300°C under inert gas environment.

Table 1. SiC Nicalon fiber properties.

Property	Value
Diameter (μm)	12–14
Density (g/cm^3)	2.55
Tensile strength (Mpa)	3000
Elastic modulus (GPa)	220
Failure strain (%)	1.4
Specific heat capacity (J/g°C)	0.71 (25°C) 1.17 (500°C)
Coefficient of thermal expansion, 10^{-6}/°C	3.2 (25–500°C)

Table 2. Main properties of the SiC/MASL composite.[14]

Property	Value
Fiber volume fraction (V_f)	0.33
Apparent density (g/cm^3)	2.50
Longitudinal elastic modulus (Gpa)	123
Poisson's ratio	0.23
Coefficient of thermal expansion, 10^{-6}/°C (20–1000°C)	
• Parallel to the fibers	3.4
• Normal to the fibers	1.7

The elastic modulus of the MASL matrix, 70–75 GPa,[13] is three times less than the corresponding value for the fibers. In such a system, matrix cracking is expected to initiate at low loads and the bridging effect is expected to be considerable.[14] Table 2 presents key properties of the composite under investigation.[15]

Specimens

Single-edge-notched beam (SENB) specimens were prepared from the SiC/MASL plates in a vertical machining center (Rambo Machinery Co., Ltd., Taiwan) using a diamond wafering blade suitable for use with hard ceramic materials (Buehler Series 5 LC Diamond, #11 – 4298, Buehler Co. Ltd., IL, USA). The same blade was used for the construction of the notches. The notch root radius obtained was *ca* 250 μm. To avoid crack tip blunting, notch root sharpness was promoted with the help of a surgical scalpel (see also Figure 2).

Table 3. SENB specimen dimensions.

Dimension	Value in mm
Specimen width, W	5.0
Specimen length, L	40
Specimen thickness, t	3.0
Support span, S	35

The preparation of the samples was performed in a manner that ensured that the external fiber plies were oriented perpendicular to the loading direction and crack propagation. Various notch lengths (α_0) were used in order to obtain notch-to-width ratios (α_0/W) of 0.4, 0.45, and 0.5. Three-point bending tests were carried out under crosshead displacement control with a rate of 0.01 mm/min, on a servo-hydraulic testing frame (MTS® 858, MTS Systems Corporation, Minnesota, USA) equipped with a 25 kN load cell. The geometrical characteristics of the SENB specimens, chosen to satisfy plane strain requirements, are given in Table 3.

Results and discussion

Formulation of generalized fracture law

In the SENB geometry testing, composite fracture is associated with the formation of a dominant macro-crack that starts at the notch root and propagates in a plane parallel to the loading plane. The total stress intensity of this system, denoted $K_P(\alpha)$, can be expressed as the sum of two contributions: the fracture toughness of the matrix, $K_{\mu,0}$, and a contribution relating to the energy dissipated during fracture, $K_\sigma(\alpha)$

$$K_P(\alpha) = K_{\mu,0} + K_\sigma(\alpha) \tag{2}$$

For very brittle matrices, such as the glass-ceramic MASL of the composite under consideration, $K_{\mu,0}$ is negligible, hence equation (2) can be rewritten as

$$K_P(\alpha) = K_\sigma(\alpha) \tag{3}$$

For the SENB geometry and plane strain conditions, $K_P(\alpha)$ as well as the differential stress intensity factor due to bridging, $dK_\sigma(\alpha, x)$, are given as a function of position x, along the crack propagation path by the following equations:[16]

$$K_P(\alpha) = \frac{3P(\alpha)S}{2tW^2} \cdot \sqrt{\pi\alpha} \cdot F\left(\frac{\alpha}{W}\right) \tag{4}$$

$$dK_\sigma(\alpha, x) = \frac{2\sigma(\delta)}{\sqrt{\pi\alpha}} \cdot H\left(\frac{\alpha}{W}, \frac{x}{\alpha}\right) \cdot \mathrm{d}x \tag{5}$$

where $\sigma(\delta)$ is the stress profile as a function of the local crack opening displacement δ, $H(\alpha/W, x/\alpha)$ is a non-dimensional factor that depends on specimen geometry as well as on the position along the crack propagation, x, and $F(\alpha/W)$ is the non-dimensional geometry correction factor for the SENB configuration. The mathematical expressions for both factors $H(\alpha/W, x/\alpha)$ and $F(\alpha/W)$ are given in the Appendix.

Equation (5) implies that calculation of the total stress intensity factor due to energy dissipation during fracture, $K_\sigma(\alpha)$, requires integration of the stress profile $\sigma[\delta(\alpha, x)]$ over the position along the crack propagation, x. The profile $\sigma[\delta(\alpha, x)]$ can be assumed equal to the analytical expression previously established for simplified geometries, equation (1), because a 1:1 correlation exists between the crack opening displacement, δ, measured in tensile tests (where δ is constant at each position along the bridging zone) and the displacement $\delta(\alpha,x)$ of the SENB geometry which varies linearly with the position x along the bridging zone. This claim is explained in the following and depicted schematically in Figure 1.

During SENB testing, crack opening displacement, δ, varies as a function of position x along the crack, α, between zero and a maximum value measureable as COD as the notched end of the specimen (Figure 1a). If this function is a simple linear equation, i.e. if the bridging zone has a triangular form, the following equation will hold

$$\delta(\alpha, x) = 2c(\alpha - x), \quad a_0 \le x \le a \tag{6}$$

where c is the slope of the crack opening displacement profile. For each displacement value, δ_{exp}, measured during SENB testing, a range of $\delta_i(\alpha,x)$ is defined with values that vary linearly between zero and δ_{exp} within the triangular bridging zone. Each of these values are directly analogous to the displacements $\delta_{exp,i}$ measured during testing of a simple tensile specimen (constant-profile bridging zone, Figure 1(b)).

Based on the above argumentation and equations (4) and (5), the following expression can be written

$$\frac{3P(\alpha)S}{2tW^2} \cdot \sqrt{\pi\alpha} \cdot F\left(\frac{\alpha}{W}\right) = \int_{a_0}^{a} \frac{2\sigma[\delta(\alpha, x)]}{\sqrt{\pi\alpha}} \cdot H\left(\frac{\alpha}{W}, \frac{x}{\alpha}\right) \cdot \mathrm{d}x \tag{7}$$

Solving equation (7) for $P(\alpha)$ leads to

$$P(\alpha) = \frac{4tW^2}{3\pi S} \cdot \frac{1}{\alpha \cdot F\left(\frac{\alpha}{W}\right)} \cdot \int_{a_0}^{a} \sigma[\delta(\alpha, x)] \cdot H\left(\frac{\alpha}{W}, \frac{x}{\alpha}\right) \cdot \mathrm{d}x \tag{8}$$

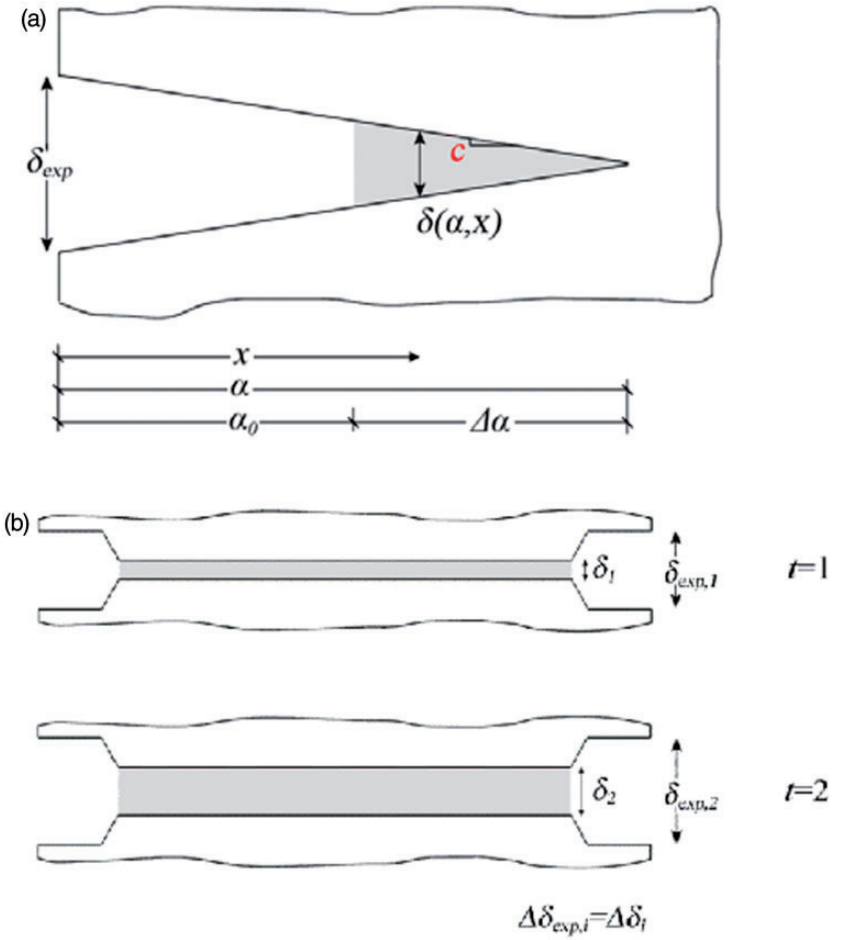

Figure 1. Geometrical relationships between the crack opening displacements, δ, in DEN(T) and SENB geometries. The bridging zone is shown in grey color. At sequential time instances, $t=1$ and $t=2$, only one dimension of a DEN(T) bridging zone changes.

If the slope c is known, the fracture law $\sigma[\delta(\alpha, x)]$ can be integrated in order to obtain the function $P(\alpha)$. If the $u(\alpha)$ function is also known, the analytical P-u curve can be calculated.

For the calculation of parameter c, i.e. the slope of the triangular bridging zone, the following methodology was adopted. During an early loading stage of a SENB specimen (in every case at instances before the maximum load was attained), the imposed crosshead displacement was paused. The instantaneous crack length, $\Delta\alpha$, and COD at $x=\alpha_0$, δ_{max} would be measured using an inline microscope with a known step-motion capability.[17] Assuming a symmetric triangular bridging zone shape (isosceles triangle), slope c was calculated from the result of the division $\delta_{max}/\Delta\alpha$.

For the calculation of the $u(\alpha)$ function, we consider that the total deflection of the SENB specimen, u, can be expressed as the sum of two contributions: a contribution associated with the beam's elastic bending, u_{el}, and a contribution related to crack propagation, u_{inel}. The primer term is given by classic theory of elasticity as

$$u_{el}(P) = \frac{PS^3}{4EtW^3} \tag{9}$$

where E is the composite's elastic modulus in the longitudinal direction. The inelastic contribution has been calculated as[18]

$$u_{inel}[\delta(\alpha, x)] = \frac{3S}{W^2}\int_0^{\alpha}\left(1-2\frac{x}{W}\right)\cdot\delta(\alpha, x)\cdot \mathrm{d}x \tag{10}$$

Then, function $u(\alpha)$ can be written as

$$u(\alpha) = \frac{PS^3}{4EtW^3} + \frac{3S}{W^2}\int_0^{\alpha}\left(1-2\frac{x}{W}\right)\cdot\delta(\alpha, x)\cdot \mathrm{d}x \tag{11}$$

Having experimentally established functions $P(\alpha)$ and $u(\alpha)$ by integration of the crack opening function

$\delta(\alpha, x)$ as per equations (8) and (11), the analytically-expected $P(u)$ behavior of each SENB specimen is theoretically feasible by function composition. However, due to the complexity in the expressions for the $F(\alpha/W)$ and $H(\alpha/W, x/\alpha)$ factors, it was not possible to establish an analytical expression for $P(u)$ by elimination of crack length α between $P(\alpha)$ and $u(\alpha)$ (equations (8) and (11)). The theoretical $P(u)$ curves were alternatively constructed by interrogation of discrete experimental values. The total crack length was divided into a large number of discrete segments, and for each crack length value, a P and u value was calculated from equations (8) and (11). In this manner, pairs of $P(u)$ are obtained for each α.

The fracture behavior of the particular composite has been found to be consistent with the formation of a dominant macrocrack that starts at the notch root and propagates within the material to give rise to intefacial debonding, fiber bridging, sliding, and pull-out.[14,17] The behavior was verified for the SENB geometry of the current study by post-mortem observations of the failed ligaments of the samples after three point bending tests. As seen in Figure 2, material fracture is associated with the formation of a dominant macrocrack around which energy dissipation mechanisms such as fiber bridging and pull-out evolve. This observation in combination with the absence of delamination validate the applicability of the established formulation to the fracture behavior of the composite under investigation.

Figure 3 represents typical experimental load versus beam deflection (P-u) curves of SiC/MASL SENB specimens with three different notch-to-width ratios, plotted against the analytically expected counterparts. The material properties entering equations (8) and (11) have been established earlier for the specific SiC/MASL composite[12] and are presented in Table 4. It is observed that the theoretically expected behavior that incorporates the generalized fracture law closely approximates the experimentally recorded values for the biggest part of the curve. However, it is obvious that the model cannot follow the experimental data at deflections larger than 0.45–0.5 mm. This is because the behavior observed in this regime is related to the naturally expected compressive zone that develops on the back face of SENB specimens. Such a feature has not been accounted for in the analysis, hence neither equation (8) nor equation (11) is expected to be able to assess it. The most important conclusion that can be drawn from the observed agreement between the experimental and analytical P-u curves concerns the geometry-invariance of the fracture law. If the fracture law is successful in assessing the fracture behaviors of two independent specimen geometries with completely different damage zones and crack opening scenarios, such as the DEN tension specimen and the SENB specimen, then it is a

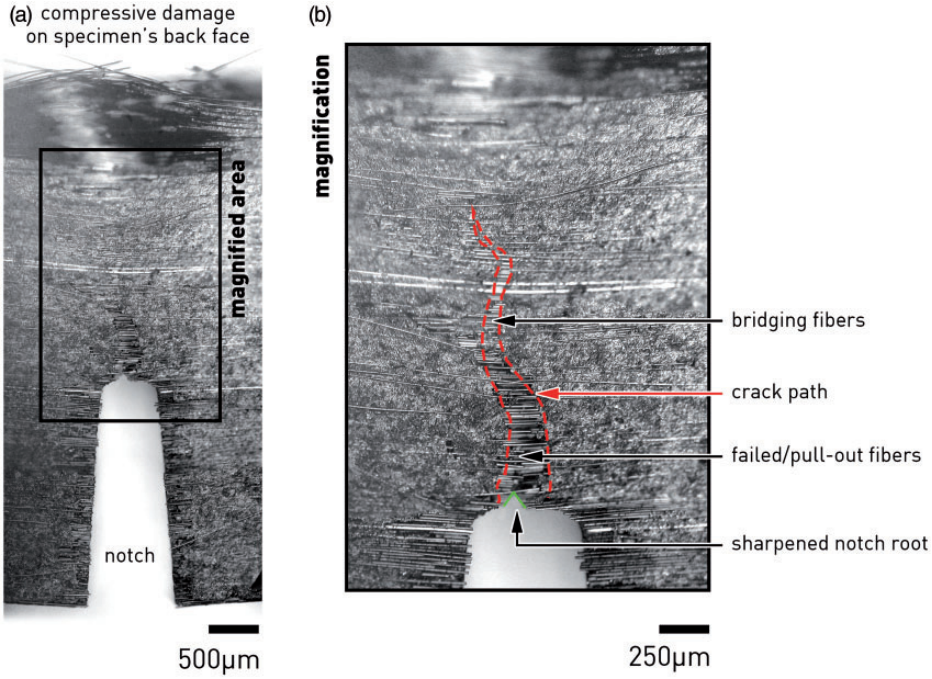

Figure 2. Post-mortem micrographs of the failed ligaments of SENB SiC/MASL samples. (a) micrograph of whole ligament illustrating notch, damage zone, and bending-bound compressive damage on back face. (b) Magnified micrograph of damage zone illustrating dominant macrocrack and fiber bridging, pull-out, and crack deflection.

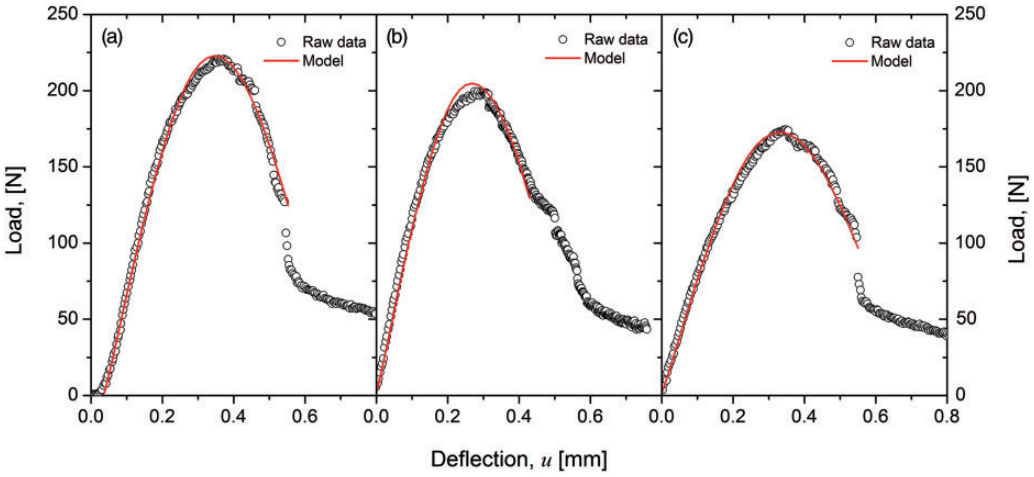

Figure 3. Comparison of modeled *P-u* fracture laws across raw experimental data for SENB specimens with $W = 5.3$ mm and three different notch-to-width ratios: (a) $\alpha_0/W = 0.4$, (b) $\alpha_0/W = 0.45$, and (c) $\alpha_0/W = 0.50$.

Table 4. Material and specimen properties required by the analytical fracture law.

Parameter	Value
Specimen parameters	
$l = S$ (mm)	35
R_f (μm)	7
V_f (−)	0.35
Fibre properties	
E_f (GPa)	207.9
k (−)	0.5
a_f (−)	2.528
b_f (mm)	0.0952
δ^* (mm)	0.0193
Matrix properties	
E_m (GPa)	69.5
a_m (−)	1.889
b_m (mm)	0.0366
Interface properties	
τ (MPa)	3.04
L_p (μm)	570

geometry-, hence also dimension-invariant relation that constitutively governs the fracture of the CMC material under investigation. Such a relationship can be used as a standalone tool for predicting material damage without the need of testing. The proposed law can, however, assess only those fracture behaviors that exhibit the energy dissipation mechanisms it assumes; for example it cannot be used to predict fracture under compressive loads where failure is governed by shear mechanisms and buckling of fiber blocks. The potential of the established law as a prediction tool is investigated in the following.

Fracture law as a prediction tool

For design and modeling purposes, it is relevant to examine whether the geometry-invariant fracture law is also successful in *a priori* predicting the load-displacement curves of hypothetical materials with similar fracture characteristics as the composite under investigation. In fact, if all parameters entering equations (1) and (8) are known for a specific system, the analysis can provide a valid load–displacement behavior, possibly rendering characterization through mechanical testing unnecessary.

To demonstrate this potential, the law was used to predict the mechanical response of three hypothetical scenarios relating to composite systems with different energy dissipation capacities. In the first case, the material is assumed to exhibit negligible bridging; reinforcements fail massively within the matrix soon after matrix cracking completes. The system is modeled by employing a large Weibull shape parameter, $a_f = 20$ for the fibers, allowing for a narrow failure distribution. The second case concerns a composite with minimal energy dissipation due to pull-out, modeled using a small mean pull-out length value of $L_p = 50$ μm. The third material is a composite with strong interface and is modeled using a high value for the interfacial shear stress, $\tau = 10$ MPa. A 12-mm wide, 2-mm thick specimen with 0.4 notch-to-width ratio is assumed. The corresponding predicted load–displacement curves are shown in Figure 4.

The effect of the bridging mechanism in the overall fracture behavior of a CMC is demonstrated in Figure 4(a). The absence of the particular mechanism

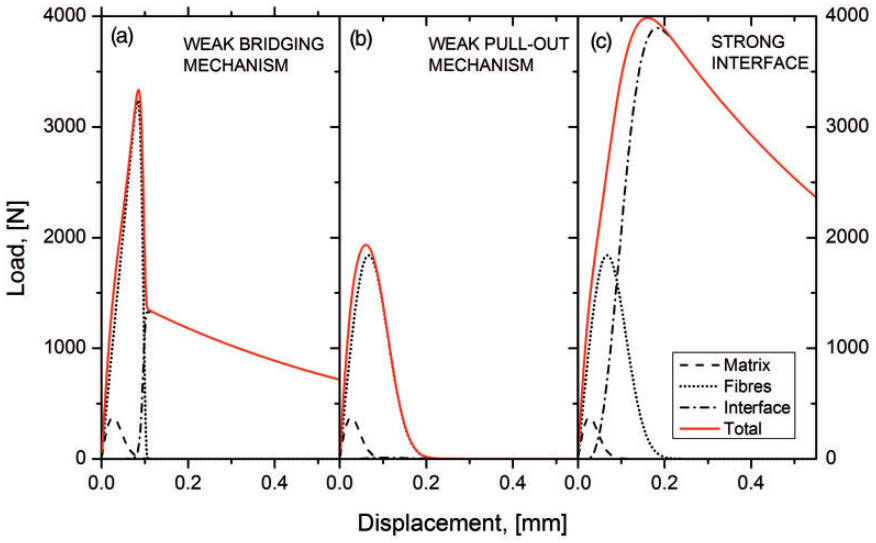

Figure 4. Predicted load–displacement curves and individual contributions of composite constituents for materials with different energy dissipation characteristics.

leads to a sharp decrease in intact fibre contribution and to an almost linear-elastic mechanical behavior up to fracture. Hence, the energy dissipation potential of the bridging mechanism is critical in controlling the composite failure mode. However, since the pull-out mechanism has not been neglected, the specimen separates with progressive fibre ends disengaging from the matrix environment, giving rise to exponentially decreasing frictional forces.

The effect of pull-out on the macromechanical response of the composite is shown in Figure 4(b). The frictional ''tail'' of the curve is not present and composite load appears to decrease smoothly, as bridging fibres progressively fail within the crack flanks.

The dramatic effect of the interface on the mechanical performance of the composite is demonstrated in Figure 4(c). A three-fold increase in the value of the interfacial shear strength leads not only to a 100% increase in the maximum load but also to a radical increase in the energy dissipation potential of the material after that point. The above observations indicate the cautiousness that should be exerted when measuring and reporting composite constituents' properties, and mainly those of the interface, that control the expected performance of the model in predicting the macromechanical behavior of similar materials.

Of equally important interest for design and modeling purposes is the investigation of the effect of material properties on the composite's overall mechanical behavior as predicted by the established fracture law. Figure 5 presents the sensitivity of the macromechanical response on six major composite properties, namely fiber elastic modulus, fiber Weibull shape and location parameters, fiber volume fraction, pull-out length, and interfacial shear strength. Each property is perturbed around four different values with all remaining properties taking values from Table 4. To facilitate perception and comparison with previous plots, in each case, one of the two intermediate values corresponds to the particular composite under investigation (property value as per Table 4). These ''baseline'' behaviors are plotted in Figure 5 as solid red lines. It is observed that material strength (maximum load) is affected by all of the investigated properties while the bridging potential of the material is influenced mainly by fiber modulus and fiber Weibull parameters. On the other hand, the same parameters do not affect the pull-out potential of the material. The information contained in Figure 5 is multifaceted and the plots can be useful in property selection for developing custom materials based on design criteria. For example, an application that requires maximum energy dissipation potential around the maximum strength and small plasticity would require a combination of high elastic and weibull moduli and small pull-out lengths (Figure 5a,b,c). On the other hand, an application requiring extended ductility may require a tougher interface combined with large pull-out lengths and fibers with small Weibull modulus. A large number of analogous combinations are made possible by examining the macromechanical behaviors depicted in Figure 5.

Conclusions

A geometry-invariant law that successfully assesses the fracture behavior, at the load-extension domain, of CMCs exhibiting energy dissipation phenomena such as matrix cracking, bridging, and pull-out, has been

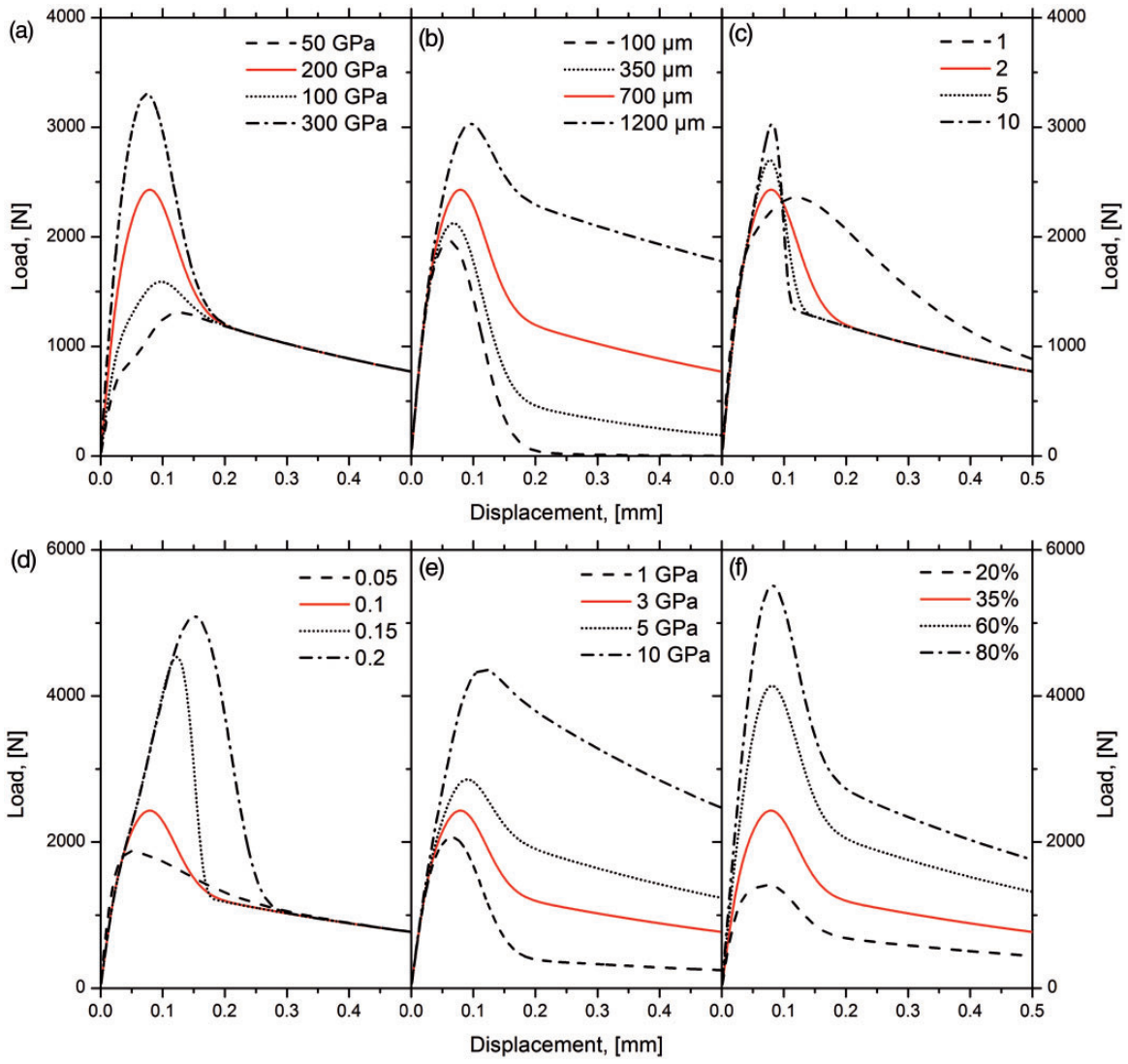

Figure 5. Sensitivity of the load–displacement behavior on (a) fiber elastic modulus E_f, (b) mean pull-out length L_p, (c) fiber Weibull modulus a_f, (d) fiber Weibull location parameter b_f, (e) interfacial shear strength τ, and (f) fiber volume fraction V_f.

analytically established and validated across experimental data of three-point bending tests on SENB specimens. The generalized fracture law is shown capable of directly assessing the original *P-u* and *P-δ* response of the material as it accounts for all energy dissipation contributions to the total behavior. Interfacial shear strength was identified as the key parameter dominating the fracture behaviour of CMCs. The fracture law was shown capable of predicting the load–displacement behavior of hypothetical CMC materials with known physical and mechanical properties. If nine specific material properties are known for a particular material system, an analytical fracture law can be obtained that renders mechanical testing unnecessary. The potential of the established law in material property selection based on application design criteria was also demonstrated.

Funding

This research received no specific grant from any funding agency in the public, commercial, or not-for-profit sectors.

Conflict of Interest

None declared.

References

1. Krenkel W and Berndt F. C/C-SiC composites for space applications and advanced friction systems. *Mater Sci Eng* 2005; 412: 177–181.
2. Brennan JJ and Prewo KM. Silicon-carbide fiber reinforced glass-ceramic matrix composites exhibiting high-strength and toughness. *J Mater Sci* 1982; 17: 2371–2383.
3. Mei H. Current development in non-destructive testing and damage evaluation for ceramic matrix composites. *Adv Appl Ceram* 2009; 108: 84–91.

4. Dassios KG, Aggelis DG, Kordatos EZ et al. Cyclic loading of a SiC-fiber reinforced ceramic matrix composite reveals damage mechanisms and thermal residual stress state. *Composites Part A: Applied Science and Manufacturing* 2013; 44: 105–113.
5. Cox BN. Extrinsic factors in the mechanics of bridged cracks. *Acta Metallurg Et Mater* 1991; 39: 1189–1201.
6. Fett T, Fünfschilling S, Hoffmann MJ, et al. Different R-curves for two- and three-dimensional cracks. *Int J Fract* 2008; 153: 153–159.
7. Dassios KG, Kostopoulos V and Steen M. Intrinsic parameters in the fracture of carbon/carbon composites. *Compos Sci Technol* 2005; 65: 883–897.
8. Foote RML, Mai YW and Cotterell B. Crack-growth resistance curves in strain-softening materials. *J Mech Phys Solids* 1986; 34: 593–607.
9. Fett T. Determination of bridging stresses and R-curves from load-displacement curves. *Eng Fract Mech* 1995; 52: 803–810.
10. Fett T. Evaluation of the bridging relation from crack-opening-displacement measurements by use of the weight function. *J Am Ceram Soc* 1995; 78: 945–948.
11. Fett T and Munz D. Bridging stress relations for ceramic materials. *J Eur Ceram Soc* 1995; 15: 377–383.
12. Dassios KG, Kostopoulos V and Steen M. A micromechanical bridging law model for CFCCs. *Acta Mater* 2007; 55: 83–92.
13. Lostec L, et al. Si-C-O fibre-reinforced ceramic matrix composites: Processing by tape casting and properties. In: *CMMC 96 – Proceedings of the first international conference on ceramic and metal matrix composites*, San Sebastian, Spain, September 09–12 1996 Pts 1 and 2. 127–123: pp.303–311.
14. Dassios KG. A review of the pull-out mechanism in the fracture of brittle-matrix fibre-reinforced cowosites. *Adv Compos Lett* 2007; 16: 17–24.
15. DrissiHabti M. Assessment of the mechanical behaviour of SiC fibre reinforced magnesium lithium aluminosilicate glass-ceramic matrix composite tested under uniaxial tensile loading. *J Eur Ceram Soc* 1997; 17: 33–39.
16. Llorca J and Elices M. Fracture-resistance of fiber-reinforced ceramic matrix composites. *Acta Metallurg Et Mater* 1990; 38: 2485–2492.
17. Dassios KG and Galiotis C. Direct measurement of fiber bridging in notched glass-ceramic-matrix composites. *J Mater Res* 2006; 21: 1150–1160.
18. Kuntz M and Grathwohl G. Coulomb friction controlled bridging stresses and crack resistance of ceramic matrix composites. *Mater Sci Eng* 1998; 250: 313–319.
19. Tada H, Paris PC and Irwin GR. *The stress analysis of cracks handbook*, 3rd ed. New York, NY: ASME Press, 2000, p.58 and p.71, 677.

Appendix

Notation

a_f	fibers Weibull shape parameter
a_m	matrix Weibull shape parameter
b_f	fibers Weibull location parameter
b_m	matrix Weibull location parameter
E_f	fibers Young's modulus
E_m	matrix Young's modulus
k	pull-out-effective fiber fraction
l	gauge length
L_p	mean pull-out length
P	load
R_f	fiber radius
S	SENB specimen support span
t	specimen thickness
u	beam deflection in 3-point bending
V_f	fiber volume fraction
W	SENB specimen width
α	crack length
α_0	SENB specimen notch length
δ	crack opening displacement
δ^*	characteristic crack opening displacement at first fiber failure
$\sigma_{br}(\delta)$	bridging stress distribution (bridging law)
$\sigma(\delta)$	generalized fracture law
τ	interfacial shear strength

Appendix

The expression for $H(\alpha/W, x/\alpha)$ for the SENB specimen geometry is given by[18]

$$H\left(\frac{\alpha}{W}, \frac{x}{\alpha}\right) = \frac{g(\alpha/W, x/\alpha)}{\left(1-\frac{\alpha}{W}\right)^{\frac{3}{2}}\sqrt{1-\left(\frac{x}{\alpha}\right)^2}} \tag{12}$$

where

$$g(\alpha/W, x/\alpha) = g_1(\alpha/W) + g_2(\alpha/W)\cdot\frac{x}{\alpha} + g_3(\alpha/W)\cdot\left(\frac{x}{\alpha}\right)^2 + g_4(\alpha/W)\cdot\left(\frac{x}{\alpha}\right)^3 \tag{13}$$

$$g_1(\alpha/W) = 0.46 + 3.06\frac{\alpha}{W} + 0.84\left(1-\frac{\alpha}{W}\right)^5 + 0.66\left(\frac{\alpha}{W}\right)^2\left(1-\frac{\alpha}{W}\right)^2 \tag{14}$$

$$g_2(\alpha/W) = -3.52\left(\frac{\alpha}{W}\right)^2 \tag{15}$$

$$g_3(\alpha/W) = 6.17 - 28.22\frac{\alpha}{W} + 34.54\left(\frac{\alpha}{W}\right)^2 - 14.39\left(\frac{\alpha}{W}\right)^3 - \left(1-\frac{\alpha}{W}\right)^{\frac{3}{2}} - 5.88\left(1-\frac{\alpha}{W}\right)^5 - 2.64\left(\frac{\alpha}{W}\right)^2 \times \left(1-\frac{\alpha}{W}\right)^2 \quad (16)$$

$$g_4(\alpha/W) = -6.63 + 25.16\frac{\alpha}{W} - 31.04\left(\frac{\alpha}{W}\right)^2 + 14.41\left(\frac{\alpha}{W}\right)^3 + 2\left(1-\frac{\alpha}{W}\right)^{\frac{3}{2}} - 5.04\left(1-\frac{\alpha}{W}\right)^5 + 1.98\left(\frac{\alpha}{W}\right)^2\left(1-\frac{\alpha}{W}\right)^2 \quad (17)$$

$F(\alpha/W)$, the non-dimensional geometry correction factor for the SENB configuration is given by[19]

$$f(\alpha/W) = \frac{\pi^{-1}/_2}{(1+2\alpha/W)(1-\alpha/W)^{3/2}} \times [1.99 - (\alpha/W)(1-\alpha/W) \times \left(2.15 - 3.93\alpha/W + 2.7^{\alpha^2}/_{W^2}\right)] \quad (18)$$